# Theoretical and experimental study of passive mode-locked optoelectronic oscillators

**Etgar C. Levy* and Moshe Horowitz**

*Department of Electrical Engineering, Technion—Israel Institute of Technology, Haifa 32000, Israel*
**Corresponding author: etgarlevy@gmail.com*

Received July 23, 2012; revised November 23, 2012; accepted November 26, 2012;
posted November 26, 2012 (Doc. ID 173056); published December 12, 2012

We present a theoretical and experimental study of passively mode-locked optoelectronic oscillators that generate a single-cycle pulse train with an autonomous envelope-carrier phase locking. The theoretical study is performed by developing a numerical simulation. A good agreement is achieved between the theoretical and the experimental results. We theoretically study the effect of the periodic frequency dependence of the dispersion coefficient on the generation of a single-cycle pulse train with an autonomous envelope-carrier phase locking. The timing jitter is experimentally measured by performing a spectral analysis of the pulse train. The spectral analysis suggests a timing jitter of about 5 ps by using an integration bandwidth of 100 Hz to 1 MHz. The measured jitter is compared to the result of the numerical simulation and to an analytical expression. © 2012 Optical Society of America

*OCIS codes:* 230.0250, 230.4910.

## 1. INTRODUCTION

The generation of ultrashort optical pulses with a duration of only a few cycles has attracted a significant amount of attention in the last few years [1–3]. Generating and measuring such short optical pulses is a challenging task. It is not possible to directly measure the electrical field of the pulses, and therefore indirect methods, such as autocorrelation measurements, are used to obtain information on the pulse envelope [2]. Such measurements give only indirect information on the pulse waveform. They also require many pulses and are based on various additional assumptions.

The common technique for generating ultrashort optical pulses is based on passive mode locking of lasers [4,5]. The duration of the generated optical pulses in passive mode-locked lasers that was demonstrated experimentally was limited to a few cycles of the carrier wave [6–8]. In such short pulses, where the pulse envelope contains only a few cycles, the relative phase between the pulse waveform and its envelope becomes significant. In general, the pulse envelope propagates at the group velocity while the carrier wave propagates at the phase velocity. As a result, the relative phase between the pulse envelope and the carrier wave may change from one round trip to another. To obtain repetitiveness between adjacent pulses, there is a need to lock the relative envelope-carrier phase [1]. In lasers, such a locking of the envelope-carrier phase was demonstrated by adding a feedback that controls the cavity length [1]. In passive mode-locked lasers, the generated optical pulse train can have an extremely low timing jitter that can be close to its quantum-limit value [9,10].

The passive mode-locking technique requires a low-loss cavity with a length that is significantly longer than the wavelength of the generated pulses. Due to the high loss in electronic transmission lines, the advantages of the passive mode-locking technique are not utilized in electronic oscillators. In coupled optoelectronic oscillators (OEOs), optical pulses propagate in an all-optical path that includes an electro-optic modulator that is fed by an electrical continuous-wave (CW) [11]. Such coupled OEOs are based on active mode locking and not on passive mode locking. In a previous work [12], we have demonstrated experimentally passive mode locking of an OEO that generates low-jitter single-cycle RF pulse train with a carrier frequency of about 650 MHz. The generated pulse train has a long-term stability with an Allan deviation of $\sigma_y(\tau_g) = 4.5 \cdot 10^{-8}\sqrt{\tau_g}$ for a gate time of $\tau_g = 4$ s. We showed that a single-cycle pulse train in which the phase and the group velocities are autonomously locked can be directly generated by this passive mode-locked oscillator.

In this manuscript we present a theoretical and experimental study of passive mode-locked OEOs. The theoretical study is important both from the physics aspect as well as from the engineering aspect. From the physics aspect, the study enables us to investigate phenomena for which the physical mechanism behind them is not well understood, such as the autonomous carrier-envelope phase locking, which was experimentally demonstrated. From the engineering aspect, the study helps one to design a passive mode-locked OEO and to optimize its performance. We present our numerical simulation for studying the passive mode-locked OEO. We obtained a good agreement between the theoretical and the experimental pulse waveforms. Our theoretical model shows that autonomous carrier-envelope phase locking is obtained due to the periodic frequency dependence of the dispersion coefficient. In the experimental study we describe our jitter measurements by performing a spectral analysis of the generated pulse train. We show that the timing jitter in our system is about an order of magnitude higher than its theoretical limit. The discrepancy between the measured timing jitter and its theoretical limit is attributed to the nonideal RF amplifier used

 

in our experiments. Thus, we believe that the timing jitter in our passive mode-locked OEO can be even further improved toward its theoretical limit by using ultra-low-noise RF amplifiers.

## 2. THEORETICAL MODEL

In this section we describe our numerical model used to study passive mode locking in OEOs. In [12] we presented our measurement results. The numerical simulation described in this manuscript helps us to study the physics of the device. We give below a brief description of the experimental setup and the main physical effects that should be theoretically modeled. We describe the numerical simulation and the parameters that were used. Then, we present a comparison between the theoretical and the experimental waveforms. A good agreement is obtained between theory and experiments. In Section 3 we use the theoretical simulation to study the effect of dispersion on the pulse generation.

### A. Description of the Numerical Simulation

Figure 1 shows a schematic description of the system that was analyzed in this manuscript. The system corresponds to the experimental setup that is described in [12]. Light from a laser is fed into an electro-optic modulator, which is used to convert RF pulses into optical pulses. The optical pulses are sent through an optical fiber and are then detected by using a photodetector (PD). The output signal is filtered, amplified by a nonsaturated RF amplifier ($G_0$) followed by a saturable amplifier with a slow saturation time ($G$), and fed back into the electrical port of an electro-optic modulator to close the loop. We model in each round trip the effect of the electro-optic modulator, the fiber delay, the photodiode, the spectral response of the filter, and the slow gain saturation of the RF amplifier. In each round trip, an effective white Gaussian noise is added to the signal at the output of the PD. This noise represents the effective noise that is added by the RF amplifiers and the PD. In our model implementation, we calculated the voltage signal at the output of the saturable amplifier, $v_{\mathrm{RF}}(t)$, for each round-trip time $\tau$. The calculation is performed iteratively. For the $n$th iteration, the propagated voltage signal, $v^n(t) = v(t - n\tau)$, is calculated from the signal $v^{n-1}(t)$.

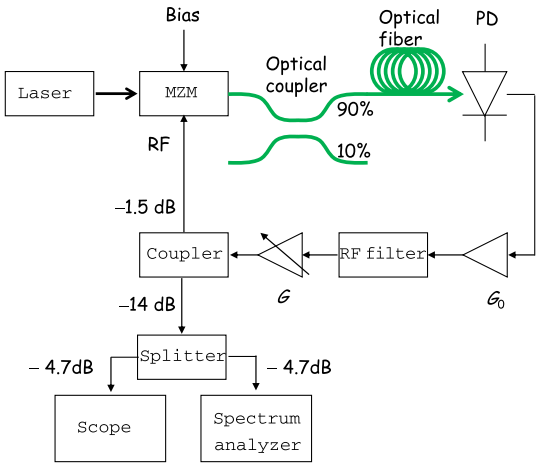


Fig. 1. (Color online) Schematic description of the experimental setup. Optical paths are represented by thick green curves and electrical paths are represented by thin black curves. Light from a continuous-wave (CW) laser is fed into a Mach–Zehnder modulator (MZM), which is used to convert an RF signal into a modulation of light intensity. The modulated light is coupled through an optical coupler to tap out 10% of the optical signal for measurements. The remaining 90% of the optical signal is sent through a long fiber, with a length of approximately 200 m, and is then detected by using a PD. The output electrical signal of the PD is amplified by a nonsaturated RF amplifier, $G_0$, which is connected to a saturable amplifier, $G$, with a maximal gain of $G_{\max} = 14$ dB. The amplified signal is fed back into the RF port of the MZM through an RF coupler. The coupler that is connected to a splitter is used to tap out –18.7 dB of the RF signal in order to measure it by both a real-time oscilloscope and an RF spectrum analyzer.

The electro-optic modulator that is modeled in our simulation is a Mach–Zehnder modulator (MZM), as used in our experimental setup. The optical power at the output of the MZM, $P_{\mathrm{mod}}(t)$, is given by [13]

$$P_{\mathrm{mod}}(t) = (\alpha P_0/2)(1 - \eta \sin\{\pi[v_{\mathrm{in}}(t)/v_{\pi,\mathrm{AC}} + v_B/v_{\pi,\mathrm{DC}}]\}), \quad (1)$$

where $v_{\mathrm{in}}(t)$ is the input voltage, $\alpha$ is the insertion loss of the MZM, $P_0$ is the input optical power, $v_{\pi,\mathrm{AC}}$ is the modulator half-wave AC voltage, $v_{\pi,\mathrm{DC}}$ is the modulator half-wave DC voltage, $v_B$ is the modulator bias voltage, and $\eta$ is a parameter determined by the extinction ratio of the modulator $(1 + \eta)/(1 - \eta)$. To generate stable pulses, the bias voltage of the modulator should be chosen in order that its transmission will be small for a small input voltage, $v \ll v_{\pi,\mathrm{AC}}$, and will increase as the input voltage increases until a saturation of the transfer curve is obtained.

The bandwidth of the experimental setup is mainly determined by the bandwidth of the saturable amplifier since the bandwidth of the other RF components is considerably wider (about 5 GHz). In our model we used the frequency response of the saturable RF amplifier that was measured by using a network analyzer. The power gain spectrum, $G(f)$, normalized to the maximal power gain, $G_{\max} = 14$ dB, is shown in Fig. 2. The measured phase response of the saturable RF amplifier between 200 and 1100 MHz equals $\varphi(f) = -2\pi f\tau_D + \psi(f)$, where $\tau_D \cong 10$ ns is an average delay that is added by the RF amplifier, and $|\psi(f)| \ll 2\pi$. The other components in the

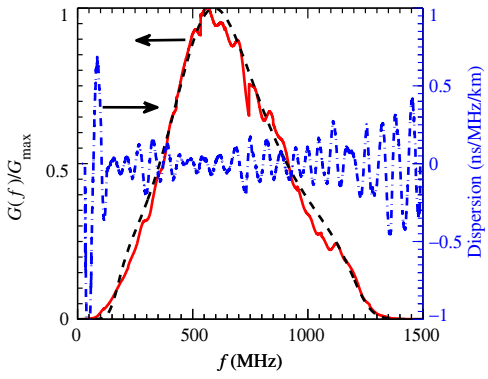


Fig. 2. (Color online) Measured frequency dependence of the power gain and the dispersion coefficient of the saturable amplifier. The measured power gain $G(f)$ (red solid curve) is normalized to the maximal power gain, $G_{\max} = 14$ dB, and the dispersion coefficient is calculated from the measured phase response according to Eq. (2) (blue dashed-dotted-curve). The measured dispersion curve shows an oscillatory structure with a period and an amplitude of about 60 MHz and 0.2 ns/MHz/km, respectively. The squared norm of the theoretical Lorenzian-bandpass filter spectral response that is described in Section 3, $|F(f)|^2$, is also shown for comparison (black-dashed curve).

cavity add a delay that is approximately equal to the delay of the optical fiber, $\tau_F \cong 938$ ns. The dispersion is calculated from the measured phase response:

$$D = \frac{1}{2\pi L}\frac{d^2\varphi}{df^2}, \tag{2}$$

where $L = 200$ m is the fiber length, and $D$ is the dispersion coefficient that is shown in Fig. 2. The dispersion coefficient has a periodic frequency dependence over a frequency octave of 440–880 MHz with a period of about $f_D = 60$ MHz and an amplitude of about $A_D = 0.2$ ns/MHz/km. We shall see in Section 3 that this oscillatory structure allows autonomous locking of the relative phase between the pulse envelope and the carrier phase that was demonstrated in the experiments. The measured frequency response of the system is represented in the theoretical model by adding an RF filter with an amplitude and a phase response that are given by $[G(f)/G_{\max}]^{1/2}$ and $\varphi(f)$, respectively.

Gain saturation with a slow response time is required to obtain mode locking [12]. In our theoretical model we have modeled the saturation curve by

$$G(t) = \frac{G_{\max}}{1 + P_{\text{avg}}(t)/P_S}, \tag{3}$$

where $G_{\max}$ is the unsaturated gain, $P_{\text{avg}}(t)$ is the low-pass-filtered RF power at the input of the saturable RF amplifier, and $P_S$ is the saturation power of the saturable RF amplifier. A comparison between the measured gain saturation curve of the saturable RF amplifier and the theoretical saturation curve that is obtained for $P_S = -22.5$ dBm is described in Fig. 3, where $P_{\text{avg}} = \langle P_{\text{in}}\rangle$, and $\langle P_{\text{in}}\rangle$ is the time-averaged RF power at the input of the RF saturable amplifier.

In our simulation we assume that the response time of the gain saturation, which is about 10 μs in the experimental setup, is much longer than the round-trip time, $T_S \gg \tau$. Thus, the low-pass-filtered RF power, $P_{\text{avg}}(t)$, at the $n$th round trip can be approximated by $P_{\text{avg}}(t) = P^n_{\text{avg}}$, where

$$P^n_{\text{avg}} = \lambda_{\text{avg}}\langle P^n_{\text{in}}\rangle_\tau + (1-\lambda_{\text{avg}})P^{n-1}_{\text{avg}}, \tag{4}$$

$\lambda_{\text{avg}} = 1 - \exp(-\tau/T_S)$ is the smoothing factor, $\langle P^n_{\text{in}}\rangle_\tau$ is the time average of the RF power at the input of the saturable amplifier over the $n$th round-trip, $P^n_{\text{in}}(t) = [v^n_{\text{in}}(t)]^2/R$, and $v^n_{\text{in}}(t)$ is the calculated voltage signal at the input of the saturable amplifier.

The parameters used in our simulation were chosen in accordance with our experimental setup: the laser input optical power was set to $P_0 = 25$ mW. The DC and AC half voltages of the MZM were set to $v_{\pi,\text{DC}} = 6$ V and $v_{\pi,\text{AC}} = 5.5$ V, respectively, the bias voltage was set to $v_B = 3.57$ V, the insertion loss was set to $\alpha = -6$ dB, and the extinction ratio was determined by setting $\eta = 0.99$. The responsivity of the PD was set to $\rho = 0.8$ A/W. The round-trip time was set to $\tau = 1$ μs and the gain of the unsaturated RF amplifier was set to $G_0 = 24$ dB. The saturable RF amplifier maximal gain was set to $G_{\max} = 14$ dB, the saturation power was set to $P_S = -22.5$ dBm, and its response time was set to $T_S = 10$ μs. We note that the bias voltage in the experimental setup was about 10 V since the transmission curve of the modulator in the experiment should be modeled by replacing $v_B$ in Eq. (1) by $v_B - v_P$, where $v_P \sim 8$ V [12].

In the numerical simulation we calculated the signal in each round trip iteratively. The result was converged after about 250 round trips. While the details of the convergence time depend on the initial conditions, the global convergence time is dominated by the slowest time response in the loop, which in our case is the slow saturation time of the RF amplifier. The saturation time of this amplifier is about 10 μs, which equals in our setup to 10 round-trip times. We simulated the propagation over a time duration of about 0.5 ms (500 round-trip times), and we have verified that the simulation results are not changed even for a longer propagation duration of 10 ms.

To evaluate the power spectral density of the noise in our system, we operated our system as an OEO that generates a CW signal by eliminating the slow saturation of the RF amplifier. Therefore, in this case we measured the phase noise when the gain of the RF amplifier is maximal. Figure 4 shows the measured phase noise of the CW signal with a carrier frequency of 625 MHz and an oscillation power of $P_{\text{OSC}} = 12$ dBm at the output of the RF amplifiers. According to [14], the phase noise of an OEO is approximately given by

$$S_\phi(f) = \frac{\delta}{(2\pi f\tau)^2}, \tag{5}$$

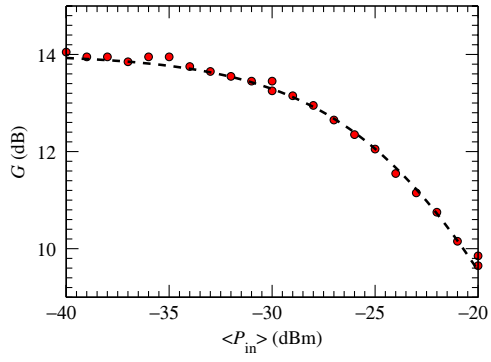


Fig. 3. (Color online) Measured gain dependence of the RF saturable amplifier as a function of the average RF input power, $\langle P_{\text{in}}\rangle$ (red circles), that is compared to the gain dependence function that was used in our numerical simulation, described in Section 2.A (black-dashed curve).

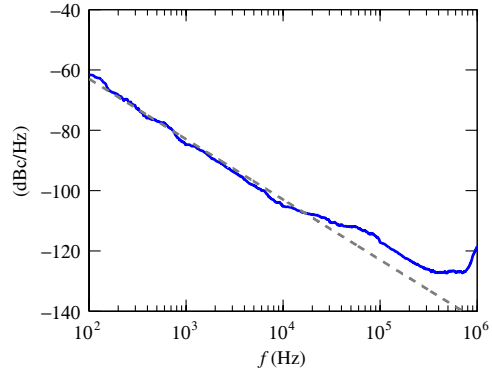


Fig. 4. (Color online) Phase-noise spectrum of our system after eliminating the saturation of the RF amplifier in order to generate a CW signal (blue solid curve). The generated signal has a frequency of 625 MHz and an oscillation power of $P_{\text{OSC}} = 12$ dBm. The theoretical phase noise calculated by using Eq. (5) is also given for comparison, using $\tau = 1$ μs and $\delta = 2 \cdot 10^{-13}$ 1/Hz (gray-dashed curve).

where $\delta = G_{\mathrm{tot}}\rho_N/P_{\mathrm{OSC}}$ is the noise-to-signal ratio and $G_{\mathrm{tot}} = 33$ dB is the total gain of the RF amplifiers. We used the relation between the phase noise and the noise-to-signal ratio, $\delta$, given in Eq. (5), and the measured phase noise shown in Fig. 4 to extract $\delta = 2 \cdot 10^{-13}$1/Hz. Therefore, the power spectral density of the noise in our numerical simulation was set to $\rho_N = 1.6 \cdot 10^{-18}$ W/Hz. We note that the $f^{-2}$ dependence of the phase noise on the offset frequency for $f > 100$ Hz, which is shown in Fig. 4, suggests the noise spectral density in our experimental setup is dominated by a white noise in this frequency region.

### B. Comparison Between Theory and Experiment

We used the numerical simulation to design our experimental setup. We obtained theoretically and experimentally a single-cycle pulse-train generation. The waveform of the generated pulses was repeated after each round trip and therefore an autonomous envelope-carrier phase was obtained in our simulation, as was obtained experimentally [12]. Figure 5 shows a comparison between the measured and the theoretically calculated single-cycle pulse waveform. A good agreement is obtained between theory and experiment. A small difference that is obtained between the theoretical and the experimental pulse tails can be attributed to a weak frequency dependence of the RF components that is not included in our model.

Single-cycle pulses were obtained in our numerical simulation when the bias voltage was in the regime $3.57 \le v_B \le 3.9$ V, such that $\pi v_B/v_{\pi,\mathrm{DC}}$ was between 1.87 and 2.04. At lower bias voltages, $v_B < 3.57$ V, no stable pulses were obtained, and at higher bias voltages, $v_B > 3.9$ V, the obtained pulses contained a few cycles. When the bias voltage was increased from $v_B = 3.57$ V to $v_B = 3.9$ V, the pulse duration increased by about 140% and the timing jitter increased by about 150%. The bias voltage in our simulation was set to $v_B = 3.57$ V, such that $\pi v_B/v_{\pi,\mathrm{DC}} = 1.87$. In this case, we obtained the minimal pulse duration as well as the minimal timing jitter.

## 3. DEPENDENCE OF THE AUTONOMOUS ENVELOPE-CARRIER PHASE LOCKING ON THE DISPERSION

In a previously published paper [12], we indicated that the periodic frequency dependence of the group velocity in the frequency region of 440–880 MHz allows the locking of the relative phase between the pulse envelope and the carrier phase in our experimental setup. This oscillation in the group velocity is caused by the periodic frequency dependence of the dispersion coefficient that is shown in Fig. 2. To study the effect of the oscillatory frequency dependence of the dispersion on the generation of a single-cycle pulse train with autonomous envelope-carrier phase locking, we studied theoretically the generation of a repetitive single-cycle pulse train for different values of the amplitude and the period of the oscillatory dispersion structure. The RF filter was modeled as a Lorenzian filter multiplied by a bandpass filter

$$|F(f)| = |\Theta(f) + \Theta(-f)| \cdot |L(f) + L^*(-f)|, \tag{6}$$

where

$$L(f) = \frac{i\Gamma/2}{f_0 - f + i\Gamma/2} \tag{7}$$

is the Lorenzian lineshape transmission, such that $f_0$ and $\Gamma$ are the central frequency and the full width at half maximum of the Lorenzian lineshape, respectively, and

$$\Theta(f) = \tanh[(f - f_{\min})/f_{\mathrm{rise},1}] - \tanh[(f - f_{\max})/f_{\mathrm{rise},2}] \tag{8}$$

is a bandpass filter transmission, where $f_{\min}$ and $f_{\max}$ are the lower and higher cutoff frequencies, respectively. To obtain an agreement between the measured and the theoretical Lorenzian-bandpass filter we used the parameters $\Gamma = 550$ MHz and $f_0 = 550$ MHz for the Lorenzian lineshape, and $f_{\min} = 150$ MHz, $f_{\max} = 1250$ MHz, $f_{\mathrm{rise},1} = 50$ MHz, and $f_{\mathrm{rise},2} = 100$ MHz for the bandpass filter. A comparison between the measured and the theoretical frequency response of the filter that was used in our simulation is given in Fig. 2. A good agreement between the squared norm of the theoretical and the measured transmission spectra is achieved. A linear phase that corresponds to a constant delay of 10 ns was added to the phase of the RF filter to obtain a casual filter response in our study. To study the effect of RF dispersion and its oscillatory behavior on the autonomous envelope-carrier phase locking, different oscillatory perturbations were added to the phase response of the RF filter:

$$\varphi(f) = -2\pi f \tau_{D,\mathrm{fil}} + 2\pi L A_D (2\pi/f_D)^{-2} \cos[2\pi(f - f_c)/f_D], \tag{9}$$

where $\tau_{D,\mathrm{fil}} = 10$ ns is a constant time delay added by the RF filter, and $f_c = 593.5$ MHz is the frequency where the transmission of the filter is maximal. We note that according to Eq. (2) the dispersion coefficient of this phase response is given by

$$D = A_D \cos[2\pi(f - f_c)/f_D]. \tag{10}$$

Thus, the dispersion coefficient has a periodic frequency dependence with an amplitude of $A_D$ and a period of $f_D$. We shall refer to $A_D$ and $f_D$ as the amplitude and the period of the oscillatory dispersion structure, respectively.

The theoretical results indicate that the maximal amplitude of the oscillatory dispersion structure that may enable a repetitive single-cycle pulse-train generation increases as the period of the oscillatory dispersion structure decreases. For example, for $f_D = 500$ MHz a repetitive single-cycle pulse train can be obtained as long as $A_D \le 0.0164$ ns/MHz/km, and for $f_D = 60$ MHz, a repetitive single-cycle pulse train can be

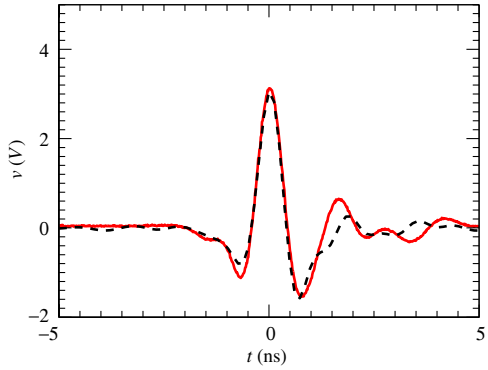


Fig. 5. (Color online) Comparison between the measured single-cycle pulse waveform (red solid curve) and the waveform that was calculated by using the numerical simulation (black-dashed curve).

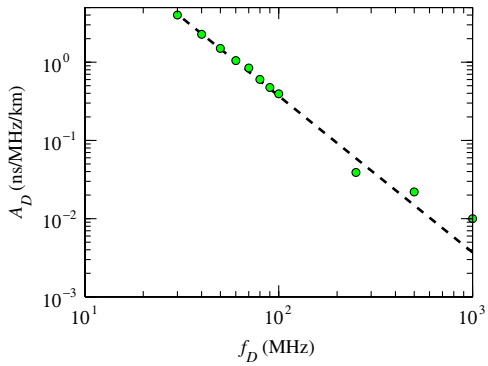


Fig. 6. (Color online) Theoretical dependence of the maximal amplitude, $A_D$, of the oscillatory dispersion coefficient defined in Eq. (8), which gives a single-cycle pulse generation on the period of the dispersion oscillation (green circles). The theoretical results are obtained when all of the simulation parameters are the same as in Fig. 5, except for the dispersion coefficient. The dependence was fitted to be $A_D = 2\pi\alpha_{\text{const}}/(Lf_D^2)$, where $\alpha_{\text{const}} = 0.12 \pm 0.01$ (black-dashed curve).

obtained as long as $A_D \le 0.969$ ns/MHz/km. In our experimental setup the oscillatory structure has a period of about 60 MHz and an amplitude of about 0.2 ns/MHz/km. For $f_D =$ 60 MHz and $A_D > 0.969$ ns/MHz/km, no mode locking was obtained in the simulations. We attribute this result to an additional effective loss that is added when the envelope-carrier locking breaks. In this case the loss in the modulator changes from pulse to pulse and it prevents the generation of a stable mode locking.

Figure 6 shows the theoretical dependence of the maximal amplitude of the dispersion coefficient, $A_D$, that enables the generation of a single-cycle pulse as a function of the period of the oscillatory dispersion structure, $f_D$. The frequency where the transmission of the filter is maximal, $f_c$, remained constant. The results were calculated by using the same parameters as in Fig. 5 unless otherwise specified. The condition under which a repetitive single-cycle pulse-train generation can be obtained can be fitted to the numerical results:

$$A_D < \frac{2\pi\alpha_{\text{const}}}{Lf_D^2}, \tag{11}$$

where $\alpha_{\text{const}} = 0.12$ is an empirical constant that may depend on other simulation parameters.

We note that the relation in Eq. (11) sets an upper bound for the value of the amplitude of the dispersion coefficient in which a single-cycle pulse generation can be obtained. A single-cycle pulse generation can be obtained for any lower value of the dispersion coefficient amplitude, $A_D$.

In case that the dispersion is small enough, a repetitive single-cycle pulse can be obtained, although there is a noticeable change in the pulse waveform at the output of the filter. This indicates that the modulator compensates the dispersion effect caused by the filter.

## 4. JITTER MEASUREMENTS

The timing jitter of the generated pulse train is determined by the noise that is added in each round trip. By using a sampling oscilloscope (Agilent Infiniium DCA-J 86100C), the measured timing jitter of the pulse train was less than 5 ps, which is approximately 5 ppm of the pulse repetition period of 948.5 ns [12]. This jitter measurement is close to the oscilloscope accuracy limit. In this section we describe the measurement of the timing jitter by using a spectral analysis of the pulse train. The experimental result is compared to theory.

### A. Spectral Analysis of the RF Pulse Train Measured by Using an Integration Bandwidth of 100 Hz to 1 MHz

The timing jitter, $\sigma_\tau$, can be evaluated by measuring the phase noise of the electrical pulse train [15,16]. Let $\xi_n$ be the $n$th harmonic normalized noise coefficient given by

$$\xi_n = 2\int_{f_{\min}}^{f_{\max}} L_n(f)\mathrm{d}f, \tag{12}$$

where $L_n(f)$ is the spectral density of the phase noise around a carrier frequency $f_n$, and $f_{\min}$ and $f_{\max}$ are the lower and higher bounds of the integration bandwidth. According to [15], the normalized timing jitter, $J = \sigma_\tau/\tau$, and the normalized amplitude noise, $A$, are related to the normalized $n$th harmonic noise coefficient, $\xi_n$, by

$$\xi_n = A^2 + (2\pi n)^2 J^2. \tag{13}$$

Figure 7 shows the measured phase noise around a carrier frequency of $f_n = 625$ MHz, which corresponds to $n = 593$. Since $n \gg 1$, the amplitude noise contribution to the value of $\xi_n$ can be neglected, and the relative jitter, $J$, can be calculated according to Eq. (13). The resulting timing jitter by using an integration bandwidth of 100 Hz (300 Hz) to 1 MHz equals $\sigma_\tau = 5$ ps (4 ps). Similar timing jitter was measured by the sampling scope Agilent Infiniium DCA-J 86100C [12] that performs a jitter spectral analysis over the region of 300 Hz to 20 MHz [17].

### B. Comparison Between Measured and Calculated Jitter

In a previous work we calculated the pulse-to-pulse jitter in our system due to additive white Gaussian noise [12]. The calculation is based on a direct contribution of white noise to the change in the central pulse time in each round trip. This calculation neglects other physical effects, such as dispersion, modulator effect, and filter bandwidth.

The numerical simulation gives a pulse-to-pulse timing-jitter with a standard deviation of $\sigma_\tau = 5$ ps for the parameters of the experimental setup. The analytic expression for the the pulse-to-pulse jitter is [12]

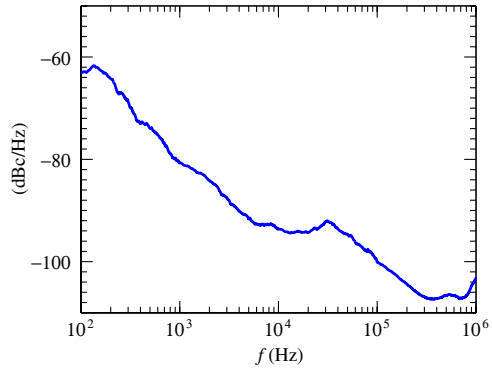


Fig. 7. (Color online) Phase noise of the generated electrical pulse train measured around a carrier frequency of 625 MHz, which corresponds to $n = 593$ harmonic order.

$$\sigma_\tau = \frac{2}{E_0}\sqrt{(G_{\mathrm{tot}}\rho_N R/2)\int_{-\tau/2}^{\tau/2} t^2 f^2(t)\mathrm{d}t}, \tag{14}$$

where $\rho_N$ is the power spectral density of the noise, $f(t)$ is the unperturbed voltage waveform of the pulse at the output of the amplifier, $G_{\mathrm{tot}}$ is the total gain of the RF amplifiers, $R$ is the load impedance, and $E_0$ is the energy of the pulse waveform

$$E_0 = \int_{-\infty}^{\infty} f^2(t')\mathrm{d}t'. \tag{15}$$

In [12] we have shown that the minimum theoretical jitter is about 0.6 ps. Here, we use in Eq. (14) the actual power spectral density of the noise that was measured in our oscillator by operating the device as a CW OEO, as described in Section 2—$\rho_N = 1.6 \cdot 10^{-18}$ W/Hz. Substituting this result in Eq. (14) gives $\sigma_\tau = 3$ ps. We have verified in the numerical simulation that the timing jitter is decreased by about 1 ps when the dispersion is eliminated, and therefore part of the difference between the analytical and the numerical results is due to the dispersion effect, which is not included in the analytical model.

## 5. CONCLUSION

A theoretical and experimental study of passively mode-locked OEOs was presented. We describe a numerical simulation that was used to develop our experimental setup and to understand the measured results. A good agreement is obtained between theory and experiments. We studied theoretically the effect of the periodic frequency dependence of the dispersion coefficient on the generation of a single-cycle pulse train with an autonomous envelope-carrier phase locking. We showed that the high-frequency oscillation of the dispersion coefficient over the pulse bandwidth allows a single-cycle pulse generation with an autonomous locking of the relative phase between the pulse envelope and the carrier wave, as it is obtained in our experiments. We measured the timing jitter by performing a spectral analysis of the pulse train. The measured timing jitter was about 5 ps for an integration bandwidth of 100 Hz to 1 MHz. The measured jitter was in agreement with the result of the numerical simulation and with an analytical expression.

## ACKNOWLEDGMENTS

This work was supported by the Israel Science Foundation (ISF) of the Israeli Academy of Sciences (grant no. 1092/10). The authors are highly grateful to Prof. C. R. Menyuk for fruitful discussions and useful remarks.

## REFERENCES

1. D. J. Jones, S. A. Diddams, J. K. Ranka, A. Stentz, R. S. Windeler, J. L. Hall, and S. T. Cundiff, "Carrier-envelope phase control of femtosecond mode-locked lasers and direct optical frequency synthesis," Science **288**, 635–639 (2000).
2. M. Y. Shverdin, D. R. Walker, D. D. Yavuz, G. Y. Yin, and S. E. Harris, "Generation of a single-cycle optical pulse," Phys. Rev. Lett. **94**, 033904 (2005).
3. G. Krauss, S. Lohss, T. Hanke, A. Sell, S. Eggert, R. Huber, and A. Leitenstorfer, "Synthesis of a single cycle of light with compact erbium-doped fibre technology," Nat. Photonics **4**, 33–36 (2010).
4. E. P. Ippen, C. V. Shank, and S. Dienes, "Passive mode locking of the cw dye laser," Appl. Phys. Lett. **21**, 348–350 (1972).
5. H. A. Haus, J. G. Fujimoto, and E. P. Ippen, "Structures for additive pulse mode locking," J. Opt. Soc. Am. B **8**, 2068–2076 (1991).
6. U. Morgner, F. X. Kärtner, S. H. Cho, Y. Chen, H. A. Haus, J. G. Fujimoto, E. P. Ippen, V. Scheuer, G. Angelow, and T. Tschudi, "Sub-two-cycle pulses from a Kerr-lens mode-locked Ti:sapphire laser," Opt. Lett. **24**, 411–413 (1999).
7. D. H. Sutter, G. Steinmeyer, L. Gallmann, N. Matuschek, F. Morier-Genoud, U. Keller, V. Scheuer, G. Angelow, and T. Tschudi, "Semiconductor saturable-absorber mirror-assisted Kerr-lens mode-locked Ti:sapphire laser producing pulses in the two-cycle regime," Opt. Lett. **24**, 631–633 (1999).
8. S. Rausch, T. Binhammer, A. Harth, F. X. Krtner, and U. Morgner, "Few-cycle femtosecond field synthesizer," Opt. Express **16**, 17410–17419 (2008).
9. H. A. Haus and A. Mecozzi, "Noise of mode-locked lasers," IEEE J. Quantum Electron. **29**, 983–996 (1993).
10. S. Namiki, X. Yu, and H. A. Haus, "Observation of nearly quantum-limited timing jitter in an all-fiber ring laser," J. Opt. Soc. Am. B **13**, 2817–2823 (1996).
11. X. S. Yao, L. Davis, and L. Maleki, "Coupled optoelectronic oscillators for generating both RF signal and optical pulses," J. Lightwave Technol. **18**, 73–78 (2000).
12. E. C. Levy and M. Horowitz, "Single-cycle radio-frequency pulse generation by an optoelectronic oscillator," Opt. Express **19**, 17599–17608 (2011).
13. E. C. Levy, M. Horowitz, and C. R. Menyuk, "Modeling optoelectronic oscillators," J. Opt. Soc. Am. B **26**, 148–159 (2009).
14. X. S. Yao and L. Maleki, "Optoelectronic microwave oscillator," J. Opt. Soc. Am. B **13**, 1725–1735 (1996).
15. D. von der Linde, "Characterization of the noise in continuously operating mode-locked lasers," Appl. Phys. B **39**, 201–217 (1986).
16. T. R. Clark, T. F. Carruthers, P. J. Matthews, and I. N. Duling III, "Phase noise measurements of ultrastable 10 GHz harmonically modelocked fibre laser," Electron. Lett. **35**, 720–721 (1999).
17. Infiniium DCA-J Agilent 86100C technical specification, http://cp.literature.agilent.com/litweb/pdf/5989-0278EN.pdf.